Analysis of Non-Canonical Body-Conformal Arrays with Polarization Decomposition

Icaro V. Soares*, Pratik Vadher*, Anja K. Skrivervik†, Giulia Sacco*, and Denys Nikolayev*
*IETR (l'Institut d'électronique et des technologies du numérique) UMR 6164, CNRS / Univ. Rennes, Rennes, France
†Microwaves and Antennas Group, École Polytechnique Fédérale de Lausanne, Lausanne, Switzerland
icaro.soares@univ-rennes1.fr, denys.nikolayev@deniq.com

***Abstract*—Conformal phased arrays can be found in many applications due to their ability to fit tridimensional surfaces and, thanks to their scanning performance, can excel planar arrays. However, most of the previously proposed analysis methods can be applied only to canonical cases and do not consider the effects of polarization. Therefore, this paper presents a closed-form formulation for analyzing antenna arrays conformal to arbitrary surfaces, evaluating the effects of the polarization components on the overall radiation performance. Besides, an on-body array conformal to the human torso surface is analyzed as a case study, and its beam scanning performance is evaluated with the developed in-house code. Finally, an amplitude tapering methodology is proposed to switch off shadowed elements and redistribute the power to the operational ones. After applying this tapering strategy, the results show that the maximum directivity is maintained, and a significant reduction in the side lobe levels is achieved.**

***Index Terms*—amplitude tapering, beam scanning, conformal array, on-body antenna, phased arrays, radars.**

I. Introduction

On- and in-body sensors are increasingly used for several applications, including sports and healthcare [1]–[4]. All these sensors necessitate antennas to communicate [5]–[7], charge, and sense [8]–[10]. Thanks to their ability to realize a 2-D map of the environment, radars have been proposed as a promising solution for electronic travel aids to help visually impaired people to increase their understanding of the surroundings and better navigate [11]. However, they are typically included in white canes and realized entirely on rigid substrates, resulting in bulky devices. To solve the portability issue, it would be necessary to replace the current generation of rigid sensors with wearable and flexible devices integrated inside clothes. Some efforts have been made to achieve a conformal wearable vest-like garment system of on-body sensors that can cover the whole upper body or may be worn under everyday clothing [12,13]. Communication components like the antenna of such a system can be made flexible and conformal to guarantee comfort and portability.

Few preliminary studies have been reported on the feasibility of single-element resonating antennas [14]–[17], phased arrays [18,19] and traveling-wave frequency scanning antennas [1,20] on flexible materials, paving the way for wearable and conformal sensors. Single-element resonating antennas do not provide reconfigurability of the radiation pattern like phased arrays and leaky-wave antennas (traveling-wave). While in contrast to leaky-wave antennas, phased arrays have the advantage of allowing for the control of all the array elements in terms of phase and amplitude, giving higher flexibility in operation. Recent studies suggested promising feeding solutions based on plasmonic waveguides that ensure proper operation even in line breakage [21].

Compared to more classical solutions where the array elements are positioned on a planar or a well-defined curved surface, for wearable applications, they will instead be placed on a non-canonical surface, whose shape will depend on the portion of the body where the array will be positioned [12,22,23]. Despite that, most methods for analyzing the radiation performance of conformal arrays in the literature are still limited and cannot be applied to arbitrarily curved structures. On one hand, conventional closed-form analysis [24,25] is not suitable once the contribution of each element is dependent on the geometric parameters of the surface and, therefore, a straightforward array factor expression cannot be defined. On the other hand, full-wave simulations are time-consuming and can be unfeasible depending on the number of antennas that compose the array.

Apart from that, up-to-date formulations for analyzing conformal arrays usually disregard some aspects that, in practice, affect the beam-scanning performance. For instance, depending on the geometric features, the polarization components seen at the steering point differ for each array element, which modifies the total radiation pattern. However, several implementations do not handle the polarization effects [26]–[28], and the ones that take it into account require error-prone preprocessing for each element [29] or do not allow the analysis of partial directivities [30].

Therefore, this paper aims to propose a generalized algorithm that allows defining in a closed form the strategy to ensure a planar wavefront normal to the steering direction. Besides, it takes into account the polarization of each element which can be either linear or circular, and its impact on the partial directivities. Moreover, an amplitude tapering technique is presented so that, for each steering direction, shadowed elements are switched off, and the amplitude is compensated in such a way that all the operational array elements contribute equally. This algorithm is then implemented and applied to a case study consisting of an array of patch antennas conformal to the human torso. Finally, this formulation allows us to examine the beam-scanning performance and provides insight

into how to synthesize arrays with maximum directivity and reduced side lobe levels.

II. Closed-Form Analysis of Conformal Arrays

A. Problem Formulation

The problem under analysis consists of an array of $N \times M$ antennas conformal to an arbitrary surface $\Sigma(x, y, z)$ in $\mathbb{R}^3$ (Fig. 1a). In the Global Coordinate System (GCS) shown in Fig. 1b, the position of the i-th element is defined by the vector $\mathbf{r}_i = (x_i, y_i, z_i)$, P is an observation point in the farfield defined by the vector $\mathbf{r}_P = (\theta, \phi)$ in spherical coordinates, being θ and ϕ the azimuth and elevation angles, respectively. Besides, the beam-scanning direction S is defined by $\mathbf{r}_S = (\theta_{scan}, \phi_{scan})$.

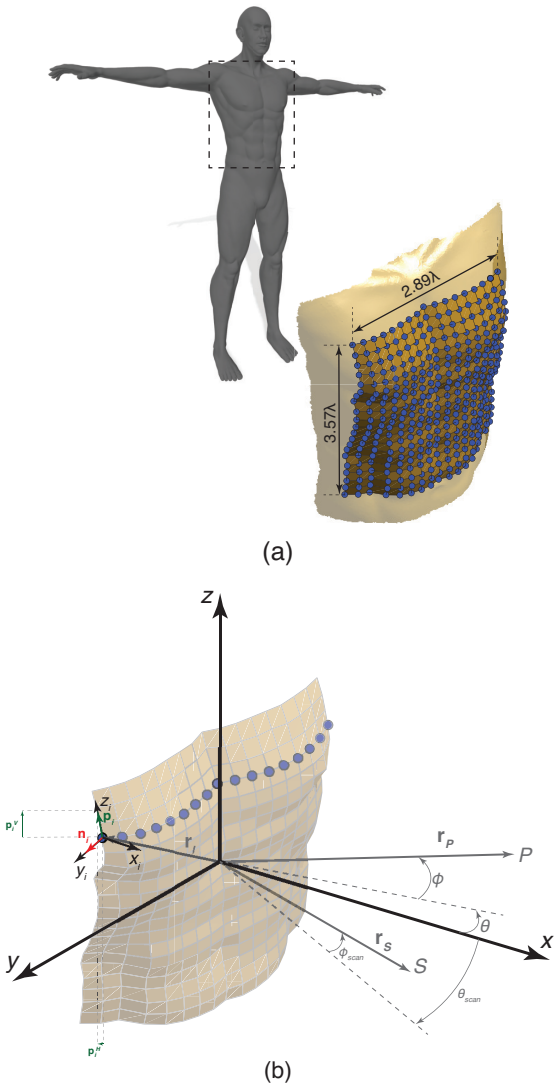

Fig. 1. On-body conformal array under analysis: (a) $N \times M$ antennas are quasi-uniformly distributed on the human torso surface, and (b) array geometry defined in a global Cartesian coordinate system $[x, y, z]$ (GCS). For the i-th element, a local system $[x_i, y_i, z_i]$ (LCS) is defined by its normal $\mathbf{n}_i$, and its polarization vector $\mathbf{p}_i$ is decomposed in vertical $\mathbf{p}_i^V$ and horizontal $\mathbf{p}_i^H$ components in GCS. The vector $\mathbf{r}_P$ defines an observation point in the farfield and $\mathbf{r}_S$ the beam-scanning direction.

The radiation pattern $\mathbf{E}(\theta, \phi)$ for any antenna array is given by the superposition of radiation pattern $\mathbf{f}_i(\theta, \phi)$ of its elements. In this way:

$$\mathbf{E}(\theta, \phi) = \sum_{i=1}^{N \times M} \mathbf{f}_i(\theta, \phi) w_i e^{-jk(\mathbf{r}_i \cdot \mathbf{r}_p)}, \tag{1}$$

in which $k = 2\pi/\lambda$ is the propagation constant for a given wavelength λ, and $w_i = a_i e^{-j\beta_i}$ are complex weights with real-valued a_i amplitude. The phase β_i of each element is defined in order to compensate for the path length difference to the beam-scanning direction S [24]:

$$\beta_i = k\left(\mathbf{r}_i \cdot \mathbf{r}_s\right). \tag{2}$$

Therefore, there is an equiphasic front perpendicular to $\mathbf{r}_S$ [27].

Once several techniques are available in the literature to mitigate the coupling between the antenna elements, the array can be designed appropriately to minimize this effect [24]. Therefore, as this paper aims to propose a rapid code, the mutual coupling is disregarded in the following analysis.

B. Coordinate System Transformation

An array of isotropic antennas whose element factor $\mathbf{f}_i$ is independent of (θ, ϕ) is sufficiently modeled by (1). However, for more general radiation patterns, it is necessary to define a Local Coordinate System (LCS) for each element. Therefore, for the i-th antenna, a Cartesian LCS is defined by placing $\mathbf{r}_i = (x_i, y_i, z_i)$ and then orienting its vector $\mathbf{n}_i = (\theta_i, \phi_i)$ normal to the surface in GCS such as shown in Fig. 1b. In this way, the transformation matrix $\mathbb{T}$ defined as [28]:

$$\mathbb{T} = \begin{bmatrix} \cos\theta_i & -\sin\theta_i & 0 \\ \sin\theta_i & \cos\theta_i & 0 \\ 0 & 0 & 1 \end{bmatrix} \cdot \begin{bmatrix} \cos\phi_i & 0 & -\sin\phi_i \\ 0 & 1 & 0 \\ \sin\phi_i & 0 & \cos\phi_i \end{bmatrix}, \tag{3}$$

can be used to evaluate any parameter defined in GCS to each LCS.

C. Polarization Decomposition in Conformal Arrays

The antenna polarization significantly contributes to the total radiation performance of the array. For instance, even though the polarization unit vector $\mathbf{p}_i$ of the i-th element shown in Fig. 1b is oriented in its local z_i axis, due to the surface curvature, its projection in GCS leads to a vertical $\mathbf{p}_i^V$ and a horizontal $\mathbf{p}_i^H$ component that must be taken into account in the superposition in (1).

Generally, if the i-th element radiation pattern in LCS is defined as $f_i\mathbf{p}_i$, its contribution in GCS is given by:

$$\mathbf{f}_i = \mathbb{T}_i^{-1}(f_i\mathbf{p}_i), \tag{4}$$

where $\mathbb{T}_i^{-1}$ is the inverse of the transformation matrix $\mathbb{T}_i$ for the i-th element. Then, the total radiation pattern can be calculated by substituting (4) into (1). Even though the polarization decomposition shown in Fig. 1b is carried out for a linearly polarized antenna, this approach can be equally applied to circularly polarized elements.

D. Radiation Performance

The radiation performance of an antenna array can be evaluated in terms of its directivity D, which is defined as the radiation intensity ratio between the analyzed array and an isotropic source in a given direction (θ, ϕ). Taking into account polarization effects, the partial directivities D_V and D_H can be defined for the respective vertical and horizontal field components [25]:

$$D_V = \frac{4\pi \left|\mathbf{E}_V(\theta,\phi)\right|^2}{(P_{rad})_\theta + (P_{rad})_\phi}, \tag{5a}$$

$$D_H = \frac{4\pi \left|\mathbf{E}_H(\theta,\phi)\right|^2}{(P_{rad})_\theta + (P_{rad})_\phi}, \tag{5b}$$

where $(P_{rad})_\theta$ and $(P_{rad})_\phi$ is the radiated power due to the components in θ and ϕ, respectively, given by the integral:

$$P_{rad} = \int_0^{2\pi} \int_0^{\pi} \left|\mathbf{E}(\theta,\phi)\right|^2 \sin\theta \, \mathrm{d}\theta \mathrm{d}\phi, \tag{6}$$

which can be numerically solved according to [25]. Finally, the total directivity D is given by the sum of the partial directivities:

$$D = D_V + D_H. \tag{7}$$

III. Case Study: On-Body Conformal Array

This work analyzes a case study of an array conformal to the human torso surface, as shown in Fig. 1a, according to the mathematical formulation proposed in Section II, which was implemented in MATLAB. This array is composed of vertically-oriented patch antennas whose radiation pattern in LCS can be modeled as:

$$\mathbf{E}_i(\theta_i,\phi_i) = \cos^2\theta_i \cos^2\phi_i \, \mathbf{z}_i. \tag{8}$$

An inter-element spacing equal to $\lambda/4$ at the frequency of 2.45 GHz was considered, which leads to low grating lobes [24] without a significant mutual coupling between elements, assuring the validity of the proposed formulation. Apart from that, as the array is backed by a ground plane, the influence of the human body can also be neglected.

The projection of the analyzed conformal array into the (θ, ϕ) plane is shown in Fig. 2, where the axes of the red ellipses represent the polarization components for each array element. As can be seen, in the regions with low curvature, the vertical component is dominant. However, the horizontal component becomes more noticeable as the curvature increases, and it becomes dominant at the extremities of the upper part of the chest.

A. Scanning Performance

The scanning performance of the conformal array under analysis is evaluated by calculating the directivity in the steering direction Dsteer in the region bounded by $-90° \leq \theta_{steer} \leq 90°$ and $-90° \leq \phi_{steer} \leq 90°$. The results for the partial directivities due to vertical and horizontal polarization components, as well as the total directivity, are presented in Fig. 3.

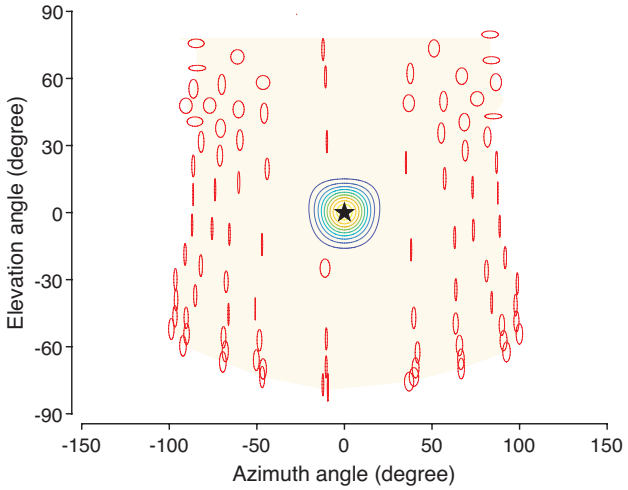

Fig. 2. Projection of the on-body conformal array into the (θ, ϕ) plane. This chart represents the vertical and horizontal polarization components of each array element as the major and minor axis of the red ellipses. The black star indicates the steering direction at the broadside, i.e., $(\theta, \phi) = (0°, 0°)$, whereas the concentric circles around it are the contour levels of the main beam.

As can be seen, the vertical component is the one that contributes the most to the overall scanning performance. For instance, a partial directivity (vertical) around 20 dBi is achieved when steering in the region $-30° \leq \theta_{steer} \leq 30°$ and $-30° \leq \phi_{steer} \leq 30°$. On the other side, the maximum directivity due to the horizontal component is around 3 dBi in the region around $\theta_{steer} = \phi_{steer} = 90°$. These results agree with the polarization behavior of each element previously discussed and evidenced in Fig. 2. The region in which the directivity due to the horizontal component reaches its maximum is on the upper extremities of the chest (around $\phi_{steer} = 90°$ and $\theta_{steer} = \pm 90°$), where the horizontal component is dominant.

The total directivity reproduces the behavior of the vertical component, except for slightly higher directivity values on the upper side corners due to the contribution of the horizontal component in this region. Apart from that, the total beam-scanning performance resembles the performance of a planar array, which is justified by the fact that the curvature radius is lower than a half-cylindrical array. However, the analyzed on-body conformal structure is able to achieve directivity values up to 16 dBi even for $\theta_{steer} \geq 60°$ and $\phi_{steer} \geq 60°$, which is not possible with planar arrays [28].

B. Amplitude Compensation

Depending on the geometry of the conformal array and the steering direction, some of its elements are shadowed, i.e., they have a low or neglectable contribution compared with the other elements. Therefore, these shadowed elements can be switched off, and the applied power can be redistributed to the others. For instance, Fig. 4a and Fig. 4b show the conformal array configuration for steering respectively at $(\theta_{steer}, \phi_{steer}) = (0°, 0°)$ and $(\theta_{steer}, \phi_{steer}) = (30°, 0°)$. The white circles represent the shadowed elements whose contribution is lower than 3 dB compared to the maximum contribution $|\mathbf{E}_{max}|$ that were switched off.

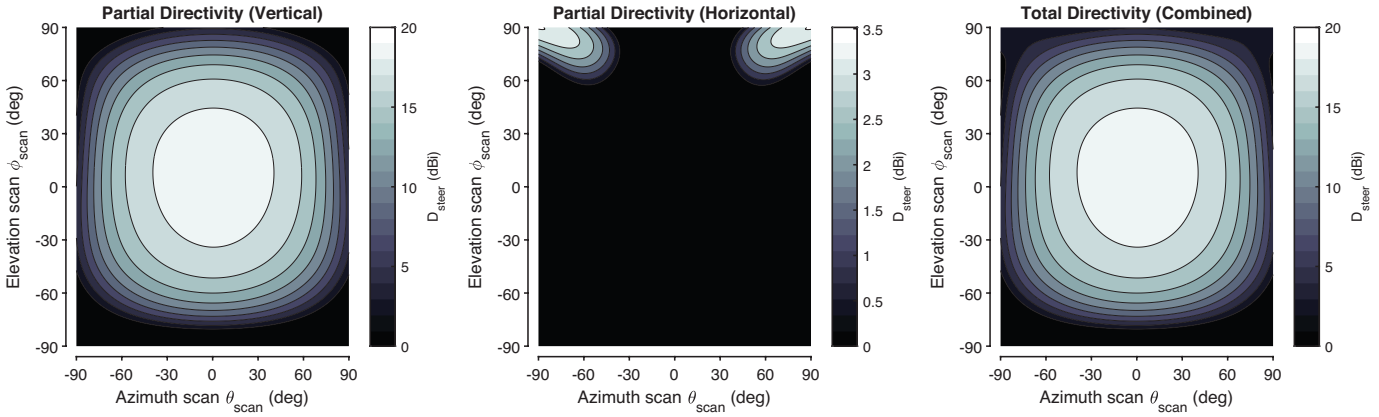

Fig. 3. Beam-scanning performance of the analyzed on-body conformal array for the vertical and horizontal polarization components as well as the combination between them. The broadside scanning direction is $(\theta, \phi) = (0°, 0°)$.

If some elements are shadowed, two approaches are possible: the freed-up power can be uniformly redistributed to the operating elements, or the amplitudes are compensated so that each element has a unitary normalized contribution given a steering direction. In other words, for the compensated array, the real-valued weight amplitude a_i of the i-th element is given by:

$$a_i = \left(\frac{\sqrt{\left|\mathbf{E}_i^V(\theta_{steer},\phi_{steer})\right|^2 + \left|\mathbf{E}_i^H(\theta_{steer},\phi_{steer})\right|^2}}{\sqrt{\left|\mathbf{E}_{max}^V(\theta_{steer},\phi_{steer})\right|^2 + \left|\mathbf{E}_{max}^H(\theta_{steer},\phi_{steer})\right|^2}} \right)^{-1}, \quad (9)$$

where $\left|\mathbf{E}_i^V\right|$ and $\left|\mathbf{E}_i^H\right|$ are the contributions of the vertical and horizontal components of the i-th element, and $\left|\mathbf{E}_{max}^V\right|$ and $\left|\mathbf{E}_{max}^H\right|$ are the maximum contributions with respect to the steering direction $(\theta_{steer}, \phi_{steer})$. Therefore, by specifying to each element a complex weight with its compensated amplitude according to (9), and its phase given by (2), a planar wavefront is seen at the steering point.

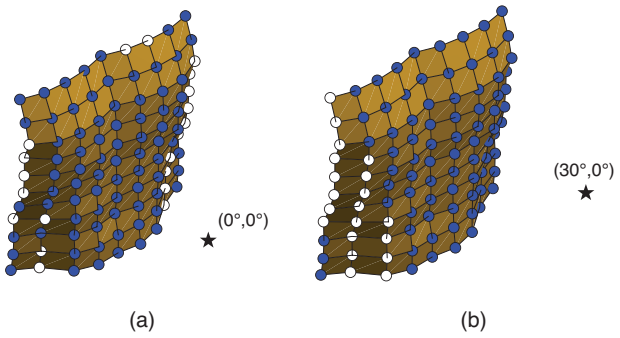

Fig. 4. Amplitude compensation for the on-body conformal array in which the elements with a low contribution ($\leq$ -3 dB) are switched off (white circles), considering the steering directions: (a) $(\theta_{steer}, \phi_{steer}) = (0°, 0°)$ and (b) $(\theta_{steer}, \phi_{steer}) = (30°, 0°)$.

The graphs in Fig. 5 show the azimuth cut of the total directivity, sampled at the elevation $\phi_{steer} = 0°$, for the cases shown in Fig. 4. The continuous blue line shows the results with elements having uniform amplitudes. In contrast, the dashed orange line shows the total directivity after switching off the elements with low contribution and applying the amplitude compensation in (9) for the operating elements. As it can be seen, even though some elements are switched off, after compensating the amplitudes, the array is able to achieve the same maximum directivity in the steering direction with a notable reduction on the side lobe levels (6.62 dBi in the best case).

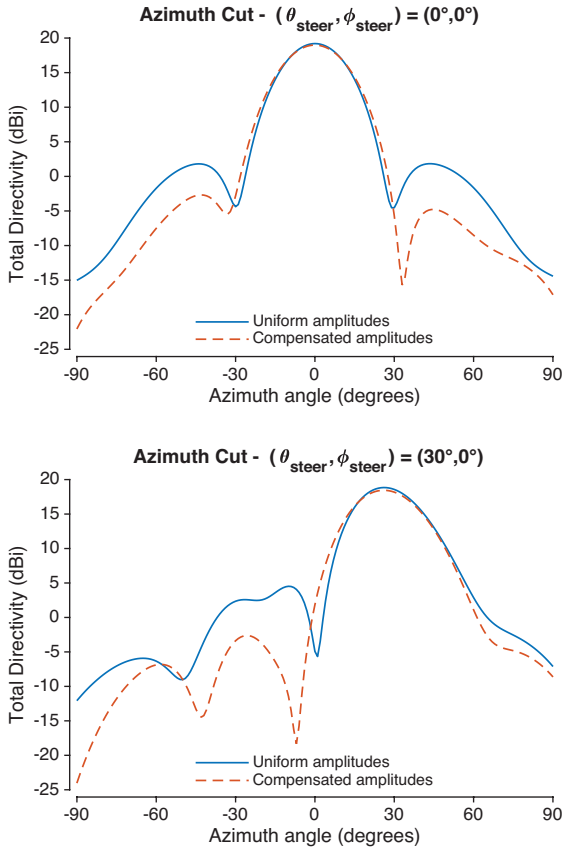

Fig. 5. Azimuthal scan of the on-body conformal array shown in Fig. 4 for 0° elevation angle. The continuous blue line is the result before element switching, with all elements with unitary amplitudes, whereas the orange dashed line is the result after amplitude compensation.

It is important to notice that the proposed amplitude compensation is a closed-form approach that could be implemented for real-time amplitude tapering, which is not possible with the time-consuming optimization methods currently in the literature.

IV. Conclusion

This paper proposes a generalized, closed-form formulation for analyzing the beam-scanning performance of phased arrays conformal to arbitrary surfaces. In this approach, the radiation pattern of each antenna is defined in its local coordinate system and then transformed into the global coordinate system in order to carry out the superposition of all contributions. This methodology can decompose the polarization of each element in its vertical and horizontal components and evaluate their impact on the overall radiation performance, being suitable for either linearly or circularly polarized antennas.

The proposed algorithm was implemented in MATLAB, and the in-house code was used to analyze an array of vertically-polarized patch antennas conformal to the human torso. The beam-scanning results show that even though the vertical component of the polarization is dominant, as the curvature increases, so does the contribution of the horizontal component. For instance, the total directivity for steering in the regions around the extremities of the upper chest is slightly increased due to the effects of the horizontal component.

Moreover, this paper presents a closed-form amplitude tapering strategy that is able to identify and switch off shadowed elements given a steering direction. Then, the amplitude of the operational elements is compensated so that all elements give the same contribution. In this way, a planar wavefront, normal to the steering direction, is formed. After applying this amplitude compensation, the results show that the maximum directivity is preserved even after switching off some elements. Besides, this tapering strategy reduces the side lobe levels without requiring time-consuming optimizations.

Even though this paper used a specific on-body conformal array as a case study, the proposed formulation and amplitude tapering algorithm can be employed to analyze and synthesize conformal arrays on any surface and with any antenna elements. Finally, for future works, it is envisaged to extend this formulation to consider the mutual coupling between the array elements.

Acknowledgment

This project was supported by the European Union's Horizon 2020 research and innovation program under the Marie Skłodowska-Curie N°899546 grant through the REACH-IT project and by the European Union's Horizon Europe research and innovation program through the Marie Skłodowska-Curie IN-SIGHT project N°101063966.

References

[1] F. Amato, C. Occhiuzzi, and G. Marrocco, "Epidermal backscattering antennas in the 5g framework: performance and perspectives," *IEEE J. Radio Freq. Identif*, vol. 4, no. 3, p. 176–185.

[2] T. He, X. Guo, and C. Lee, "Flourishing energy harvesters for future body sensor network: from single to multiple energy sources," *iScience*, vol. 24, no. 1, p. 101934.

[3] D. Nikolayev, M. Zhadobov, P. Karban, and R. Sauleau, "Conformal antennas for miniature in-body devices: The quest to improve radiation performance," *URSI Radio Sci. Bull*, vol. 2017, no. 363, p. 52–64.

[4] P. Soh, G. Vandenbosch, M. Mercuri, and D.-P. Schreurs, "Wearable wireless health monitoring: current developments, challenges, and future trends," *IEEE Microw. Mag*, vol. 16, no. 4, p. 55–70.

[5] Y. Fan, J. Huang, T. Chang, and X. Liu, "A miniaturized four-element MIMO antenna with EBG for implantable medical devices," vol. 2, no. 4, p. 226–233.

[6] S. Jilani, M. Munoz, Q. Abbasi, and A. Alomainy, "Millimeter-wave liquid crystal polymer based conformal antenna array for 5G applications," *IEEE Antennas Wirel. Propag. Lett*, vol. 18, no. 1, p. 84–88.

[7] D. Nikolayev, A. Skrivervik, J. Ho, M. Zhadobov, and R. Sauleau, "Reconfigurable dual-band capsule-conformal antenna array for in-body bioelectronics," *IEEE Trans. Antennas Propag*, vol. 70, no. 5, p. 3749–3761.

[8] J. Kim, A. Campbell, B.-F. de Ávila, and J. Wang, "Wearable biosensors for healthcare monitoring," *Nat. Biotechnol*, vol. 37, no. 4, Art. no. 4.

[9] Y. Lin, M. Bariya, and A. Javey, "Wearable biosensors for body computing," *Adv. Funct. Mater*, vol. 31, no. 39, p. p.

[10] M. Lin, H. Hu, S. Zhou, and S. Xu, "Soft wearable devices for deep-tissue sensing," p. 1–20.

[11] H. Álvarez, G. Álvarez Narciandi, F. Las-Heras, and J. Laviada, "System based on compact mmwave radar and natural body movement for assisting visually impaired people," *IEEE Access*, vol. 9, p. 125042–125051.

[12] H. Yang, X. Liu, and Y. Fan, "Design of broadband circularly polarized all-textile antenna and its conformal array for wearable devices," *IEEE Trans. Antennas Propag*, vol. 70, no. 1, p. 209–220.

[13] J. Yin, R. Hinchet, H. Shea, and C. Majidi, "Wearable soft technologies for haptic sensing and feedback," *Adv. Funct. Mater*, vol. 31, no. 39, p. p.

[14] S. Kim, "Inkjet-printed antennas, sensors and circuits on paper substrate," *IET Microw. Antennas Propag*, vol. 7, no. 10, p. 858–868.

[15] N. Chahat, M. Zhadobov, R. Sauleau, and K. Ito, "A compact uwb antenna for on-body applications," *IEEE Trans. Antennas Propag*, vol. 59, no. 4, p. 1123–1131.

[16] P. Soh, S. Boyes, G. Vandenbosch, Y. Huang, and S. Ooi, "On-body characterization of dual-band all-textile PIFA," *Prog. Electromagn. Res*, vol. 129, p. 517–539.

[17] J. C. G. Matthews and G. Pettitt, "Development of flexible, wearable antennas," in *Proc. 2009 3rd European Conference on Antennas and Propagation*, 2009, pp. 273–277.

[18] D. Anagnostou, "Flexible arrays signal change in communications," *Nat. Electron*, vol. 2, no. 5, Art. no. 5.

[19] M. Hashemi, "A flexible phased array system with low areal mass density," *Nat. Electron*, vol. 2, no. 5, Art. no. 5.

[20] P. Vadher, G. Sacco, and D. Nikolayev, "On-body V-band leaky-wave antenna for navigation and safety applications," in *Proc. 2022 IEEE Microwave, Antennas, and Propagation Conference (MAPCON 2022)*, 2012-12.

[21] X. Tian, Q. Zeng, D. Nikolayev, and J. Ho, "Conformal propagation and near-omnidirectional radiation with surface plasmonic clothing," *IEEE Trans. Antennas Propag*, vol. 68, no. 11, p. 7309–7319.

[22] D. Agrawal, "Conformal phased surfaces for wireless powering of bioelectronic microdevices," *Nat. Biomed. Eng*, vol. 1, no. 3, Art. no. 3.

[23] C. Adams, "Implementation of a skull-conformal phased array for transcranial focused ultrasound therapy," *IEEE Trans. Biomed. Eng*, vol. 68, no. 11, p. 3457–3468.

[24] R. Mailloux, *Phased array antenna handbook*, 3rd ed. Norwood, MA: Artech House.

[25] C. Balanis, *Antenna theory: analysis and design*, 4th ed. Hoboken, New Jersey: Wiley.

[26] J. Brégains, J. García-Naya, A. Dapena, and M. González-López, "A MATLAB tool for visualizing the 3D polar power patterns and excitations of conformal arrays," *IEEE Antennas Propag. Mag*, vol. 52, no. 4.

[27] H. Kobayashi, "Simple calculation method for conformal beam-scanning array pattern," in *Proc. 2019 13th European Conference on Antennas and Propagation (EuCAP)*, 2019, pp. 1–5.

[28] D. Nikolayev, A. Mazzinghi, and A. K. Skrivervik, "Rapid analysis of arbitrary-shaped conformal beam-scanning arrays," in *Proc. 2020 14th European Conference on Antennas and Propagation (EuCAP)*, 2020, pp. 1–4.

[29] M. G.-L. J. C. Brégains, J. A. García-Naya and L. Castedo-Ribas, "A MATLAB interface for analyzing conformal arrays composed of polarized heterogeneous elements,," *IEEE Antennas Propag. Mag*, vol. 53, no. 5, Art. no. 5.

[30] MathWorks, "Phased array system toolbox." [Online]. Available: www.mathworks.com/products/phased-array.html